J. Fluid Mech. (1996), *vol.* 329, *pp.* 103–115

Development of structure within the turbulent wake of a porous body. Part 1. The initial formation region

By Z. HUANG AND J. F. KEFFER

Department of Mechanical Engineering, University of Toronto, Toronto, Ontario, Canada M5S 1A4

(Received 15 January 1995 and in revised form 16 June 1996)

This paper deals with the initial region ($x/d = 1$ to 20) of a turbulent wake generated by a mesh strip. The purpose of the study is to identify the formation mechanism of the large-scale vortices which have developed by the end of this zone. The region is characterized by the evolution and interaction of two parallel shear layers generated at the edges of the mesh. Multi-point hot-wire velocity measurements establish that the merging and interaction of the small-scale eddies account for the formation of the large-scale vortices. A numerical simulation based on a discrete vortex method was carried out to gain further insight into the interaction between the two shear layers. Both the experimental and numerical results suggest that low-frequency perturbation plays an important role in the communication between the two shear layers.

1. Introduction

Recent studies (Castro 1971; Bevilaqua & Lykoudis 1978; Inoue 1985; Louchez, Kawall & Keffer 1987; Wygnanski, Champagne & Marasli 1986; Zhou & Antonia 1994) have indicated that the detailed behaviour of a turbulent wake flow, in terms of its measured statistical properties and entrainment characteristics, is strongly dependent, both in the early stages of its evolution and in its eventual self-preserving state, upon the type of body which produces the wake. Among the many types of wakes, a significant difference can be found between flow generated by a solid body (e.g. flat plate) and a porous body (mesh screen). Within the porous-body wakes, evidence (Castro 1971) also suggested that the flow characteristics may have differences according to its porosity. The distinction arises from the different eddy formation mechanism in the early stages of the flow. While the formation mechanism has been studied quite extensively for solid-body wakes (e.g. Cantwell & Coles 1983; Perry & Steiner 1987), there are still questions concerning the very near region of a porous-body wake.

Available evidence (Wygnanski *et al.* 1983; Cimbala, Nagib & Roshko 1988) suggests that the shear layers generated at the edges of a strip of screen undergo a local instability process. This generates small-scale eddies in a region very close to the screen. At a certain distance downstream, large-scale eddies emerge. There have been different explanations for the formation mechanism of the latter vortices. Cimbala *et al.* (1988) suggested that they are the result of an instability associated with the mean U velocity profile. Wygnanski *et al.* (1986), however, suggested that it is not clear whether they are due to the instability or to the growth of the small-scale vortices via entrainment or amalgamation. In general, it is not clear how this happens. Are the large and small

eddies related? If so, are the large motions formed from the amalgamation of the small eddis, or formed independently from an instability mechanism due to the mean velocity profile?

The present work concerns an experimental and numerical investigation of the formation region of the plane turbulent wake generated by a mesh strip. The main objective of the work was to determine how the coherent structures develop, which appears to have happened by about $x/d = 24$. Specifically, we are trying to answer two questions: (i) is there a relation between the high-frequency activity in the zone very close to the mesh and the large-scale structures found in downstream region, and (ii) how do the shear layers from the two edges interact with each other?

2. Experimental details

The experiments for this investigation were performed in the variable-speed low-turbulence recirculating wind tunnel in the UTME (University of Toronto, Mechanical Engineering) Turbulence Research Laboratory. This tunnel has a test section 4 m in length of 0.91 m by 1.2 m in cross-section and a speed range of about 1 m s^{-1} to about 20 m s^{-1}, with a background turbulence intensity level of about 0.05%. The wakes were generated by means of a mesh strip with a solidity of 60%. The mesh strip was made of stainless-steel wire screen, which has 24×24 wires per square inch and a wire diameter of 0.38 mm. The Reynolds number based on the wire diameter is 230. Detailed data on the screen can be found in Zucherman (1988). The width (d) of the wake generator was 18 mm and the length (L) 0.91 m, giving an aspect ratio (L/d) of approximately 50. A free-stream velocity (U_0) of 10.2 m s^{-1} was used, so that the Reynolds number based on d was about 11000.

A Cartesian coordinate system was used, with x in the streamwise direction, y in the lateral or vertical direction and z in the spanwise direction (parallel to the axis of the wake generator). The origin of the coordinate system was the centre of the wake generator. Multi-point measurements were taken in the vertical centreplane of the flow ($z = 0$). A vertical rake of X-wire probes, aligned parallel to the y-axis was used for the velocity measurements. For measurement of the wake beyond $x = 5d$, eight streamwise velocity (U) signals and eight lateral velocity (V) signals were measured simultaneously with eight DANTEC 55P61 45° X-wire probes, in conjunction with DANTEC 55M & 56C constant-temperature-anemometer systems. Each signal was low-pass filtered at 2 kHz and digitized by means of a 12-bit A/D converter. The digitization rate was chosen to be 6250 points per second for each signal. For measurements with $x \leqslant 5d$, two X-wire probes were used. The low-pass filter was set at 5 kHz and the digitization rate was chosen to be 8000 points per second. At the further upstream location of $x = 1d$, a digitization rate of 12000 points per second was used. All digital signals were stored on an optical disk and subsequently processed on a SUN SPARC2 workstation. The length of each signal processed was approximately 40 s.

3. Experimental results

3.1. *Statistical characteristics and general features of the porous-body wake*

A schematic of the porous-body turbulent wake flow is given in figure 1. For the velocity measurements taken at different positions in this wake, typical segments of the lateral velocity (V) record obtained at several points are also presented. These signals are plotted to the same scale and significantly different characteristics can be identified

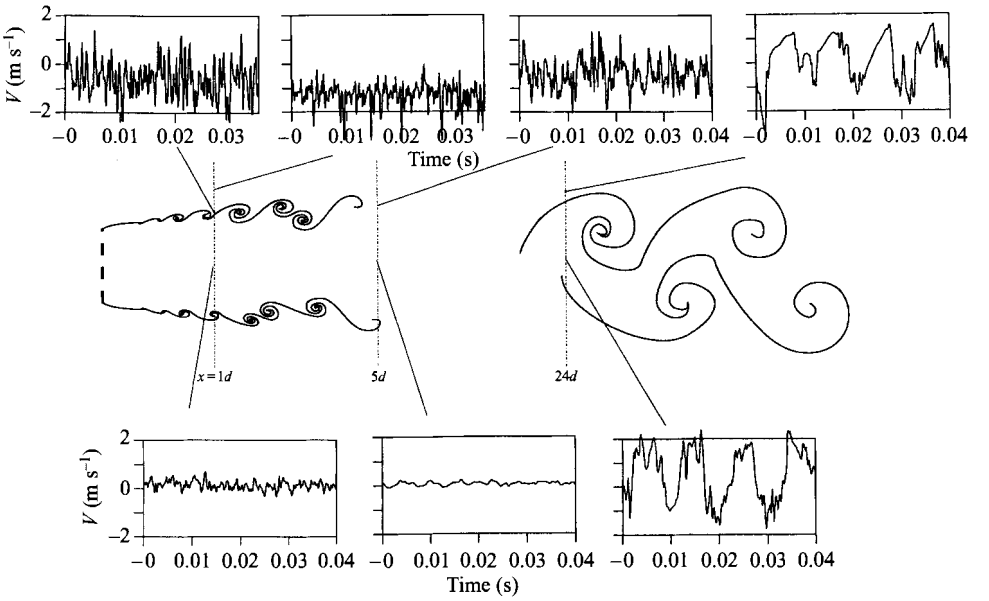

FIGURE 1. Vortices and V-velocity signals in a porous-body wake. The sketch shows the streaklines from the two edges. Velocity signals are plotted on the same scale.

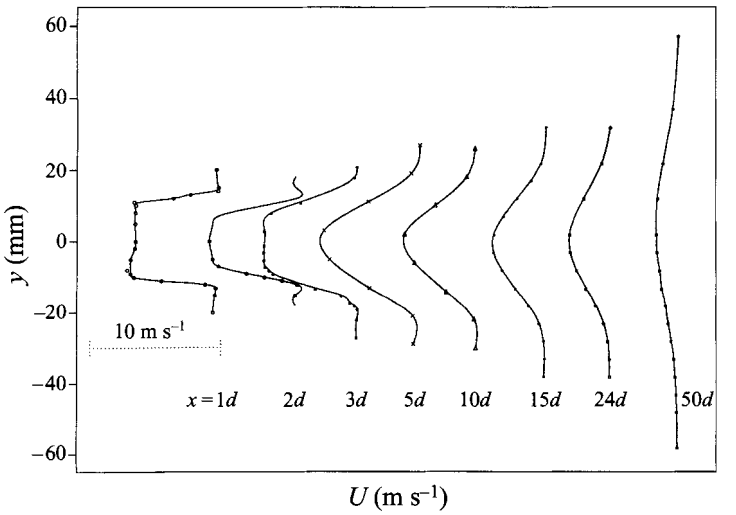

FIGURE 2. Mean U-profiles in the wake of a porous body.

for the various locations. Mean streamwise velocity profiles are shown in figure 2, and the corresponding r.m.s. lateral velocity profiles are presented in figure 3 to provide the statistical characteristics.

In the very early stage of the wake evolution, i.e. very close to the generator ($x \leqslant 2d$), the mean velocity profiles show steep velocity gradients in the shear layer on each side of the wake, separated by an essentially uniform distribution in the central portion. The shear-layer velocity signals exhibit strong fluctuations at high frequencies, as can be seen from the V-signals in figure 1. These arise from the initial instability and subsequent roll-up of the vortex sheet. In contrast, the central region of the wake,

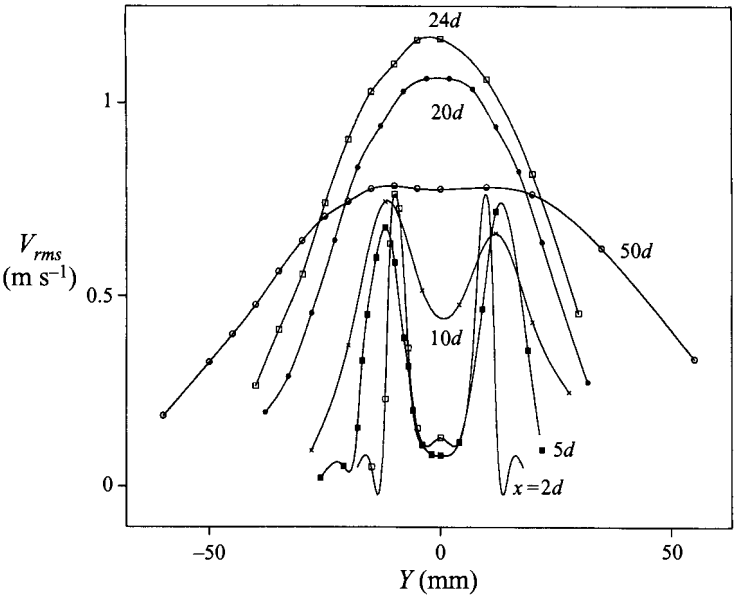

FIGURE 3. *R.M.S. V*-profiles in the wake of a porous body.

where the mean velocity is approximately uniform, is essentially a grid-generated turbulent flow. Correspondingly, the velocity fluctuations in this region are much lower than those in the shear layers.

As the flow moves downstream (to about $5d$), the originally sharp velocity gradients become relatively smooth as the shear layers grow in the lateral direction. Within the shear layers, the r.m.s. values increase, reflecting the intensifying activity within the intermittent region. In the central region, the r.m.s. values decrease in the initial stage of the development ($x < 5d$), due to viscous diffusion within the homogeneous turbulent fluid which has penetrated the screen. These r.m.s. values then increase at further downstream locations ($x > 5d$), as the two shear layers begin to interact. The measurements also show that the lateral velocity (V) is more sensitive to this disturbance than the streamwise velocity (U). The uniform portion of the mean velocity profile disappears beyond about $x = 10d$.

Figure 4 shows the U-microscale profiles at several streamwise locations. The microscale of a fluctuating velocity is expressed as

$$\lambda = \left[\frac{1}{2}\frac{1}{(\mathrm{d}^2\rho_{uu}/\mathrm{d}\tau^2)_{\tau=0}}\right]^{1/2}$$

and is an indication of the smallest scales of turbulent motion in the flow. In the region close to the centreline of the wake, the microscale increases progressively as x increases up to $8d$. This comes about because of the viscous diffusion in the region. But the microscale in the shear layers grows very slowly and maintains a considerably lower value in the same range of x.

In summary, we see that the central core of the wake flow and the two shear layers may be regarded as distinct entities. The shear layers are characterized by a strong velocity gradient and high velocity fluctuations. They contain both large scales and very small-scale turbulent motions. Because of this energetic motion, the shear layers can be expected to play an active role in the subsequent development of the wake. The

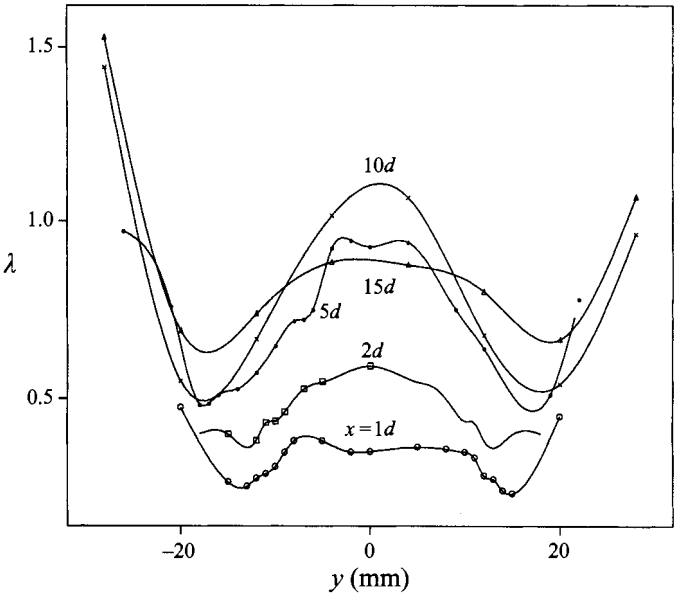

FIGURE 4. *U*-velocity microscale profiles in the wake of a porous body.

central core region acts initially as a buffer layer separating the two shear layers. Such a buffer layer is absent in other wake flows (e.g. the wake generated by circular cylinder), and is a unique feature of the present porous-body wake.

3.2. *Origin of the large-scale coherent structures*

As indicated from the signal traces in figure 1, the velocity fluctuations have a very high-frequency content in the region close to the mesh and a relatively low-frequency content in the downstream region. Spectral analysis was performed on the signals measured at different positions in the flow. Figure 5(*a*) shows the v (lateral velocity)-autospectra at different positions along the centreline of the wake. Figure 5(*b*) shows the v-spectra within one of the shear layers, close to the position where the maximum r.m.s. occurs. Figure 5(*c*) shows the v-spectra along the edges of the wake. Significant differences can be seen in the spectra both at different streamwise locations and at different lateral (y) positions. We note that the u (streamwise velocity)-autospectra are similar to the corresponding v-autospectra, except that the peaks are less prominent.

The autospectrum in the central region very close to the screen (figure 5*a*, $x = 1d$) is relatively flat up to a fairly high frequency (400 Hz), with no significant energy concentration in any specific frequency band. This is consistent with grid-generated turbulence where the turbulence energy is uniformly distributed among different length scales of the motion. A broad-band spectral peak emerges later, beyond $x = 3d$. On the other hand, the v-spectrum in the outer edge of a shear layer (figure 5*c*) contains a distinct broad-band peak of about 1000 Hz at $x = 1d$, signifying that some frequency-centred activity occurs within the shear layers. This must arise from the Helmholtz instability of the vortex sheets generated at the edges of the screen and the subsequent roll-up of these sheets into discrete vortices, in a similar fashion to the single shear layer development discussed by Roshko (1976). The nominal frequency associated with the peak in the spectrum represents the characteristic frequency of these vortices.

From a comparison of the spectra at $x/d = 1$ and 2 in figure 5(*c*), it can be seen that the characteristic frequency of the vortices changes from 1000 Hz to about 600 Hz. It

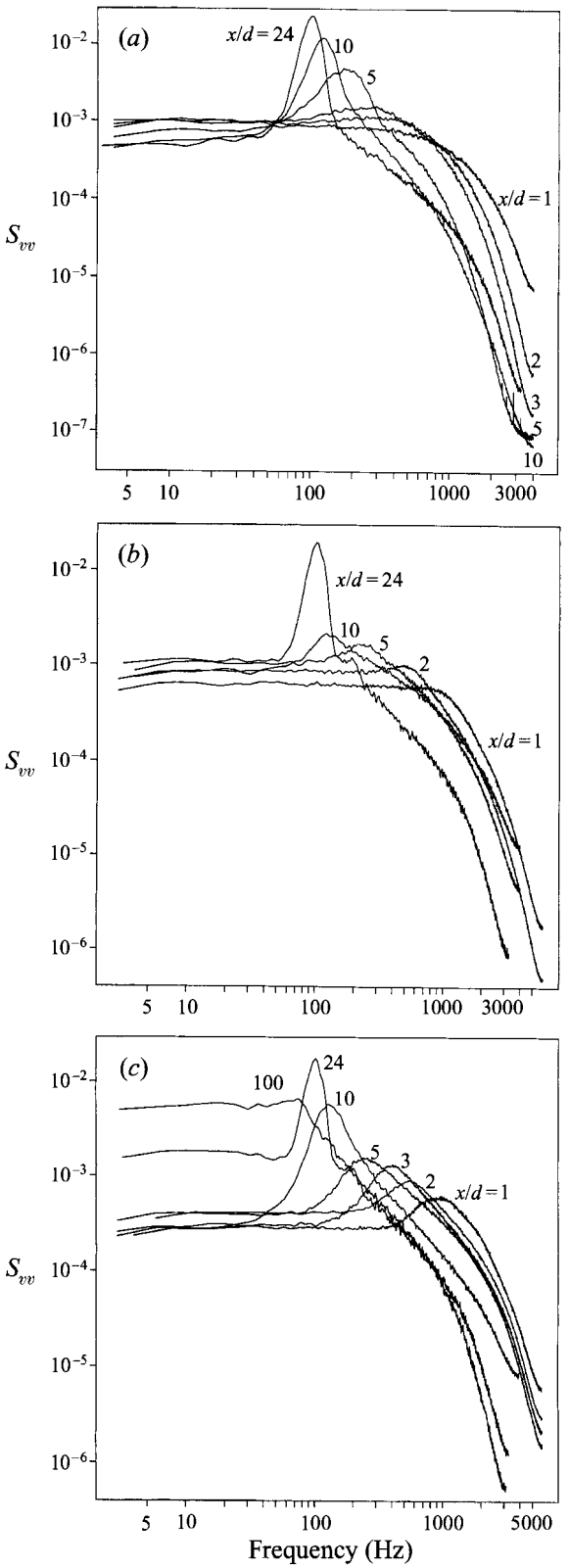

FIGURE 5. Autospectra of v: (*a*) along the centreline of the porous-body wake: (*b*) within the shear layer of the porous-body wake; (*c*) along the outer edge of the porous-body wake.

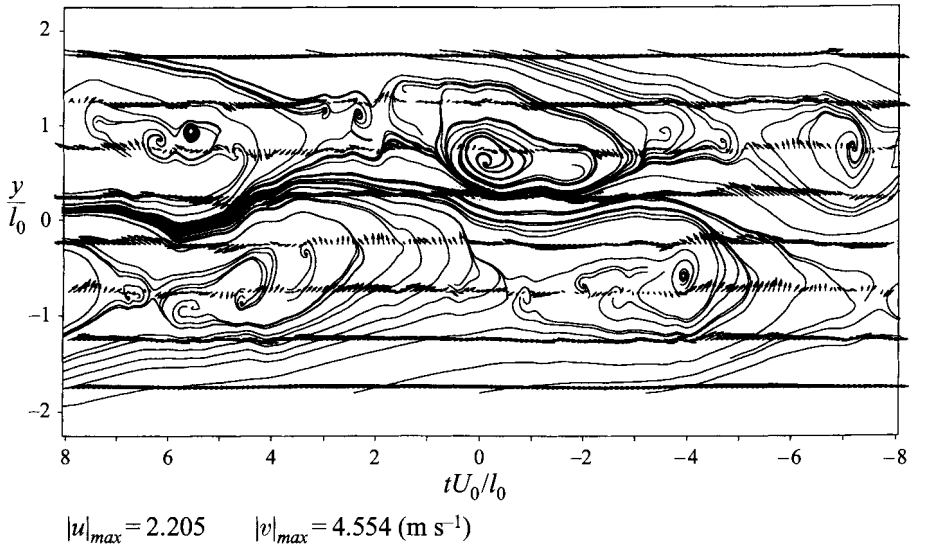

FIGURE 6. 'Instantaneous' realization of u- and v-velocity vector and streamline patterns at $x = 15d$.

is inferred from this that the vortex sheets have already rolled up at $x = 1d$ and the resulting vortices have undergone an evolution within the shear layers by $x = 2d$. The variation of this characteristic frequency along the streamwise direction shows that the vortical structures grow within the shear layers.

It should be emphasized that in the formation region of the present wake flow ($x = 1d$ to $24d$), each v-spectrum in figure 5(c) displays a broad-band peak, indicating that periodicity exists at all stations. In addition, the results show that, as the flow moves downstream within this region, the periodicity becomes progressively stronger and the characteristic frequency of the spectral peak decreases to about 100 Hz at $x = 24d$. The Strouhal number ($S = fd/U_0$, where f is the characteristic frequency at $24d$) is about 0.188 and is close to the measurement made by Castro (1971), for a porous-body wake of 40% porosity. This evidence suggests that eddies generated in the formation region of the shear layers persist throughout the flow region of $x = 1d$ to $20d$. Instead of a gradual decay due to the viscosity, these eddies appear to become stronger, as seen by the velocity signals. From this we can infer that vortex merging is taking place.

Further evidence supporting the vortex merging process is provided by figure 6. This is an 'instantaneous' realization of velocity vectors at $x = 15d$, obtained via a rake of eight X-wire probes. A streamline pattern, based on the interpolation and integration of the measured velocities, is superimposed on the velocity vectors. (In this figure, l_0 and U_0 represent the half-width of the wake at $x = 24d$ and the free-stream velocity respectively. The frame is assumed to move at a reference velocity equal to the averaged velocity in the shear layers, i.e. $0.735U_0$.) We note that several foci (points with spiral streamlines) can be identified from the streamline pattern. Clearly these are the points around which the fluid rotates and we may think of this as the centre of a vortex.

The results in figure 6 establish that vortices have been created within the shear layers. But they also indicate that these vortices can have a range of sizes. The latter can be estimated from the radii of the streamlines that enclose the focal points. Moreover, the figure suggests that more than one focus can be enclosed by a 'larger' streamline, i.e. two or three small vortices may be the basis of a larger vortex. The spacing between such large structures is roughly equal to the spacing based on the characteristic

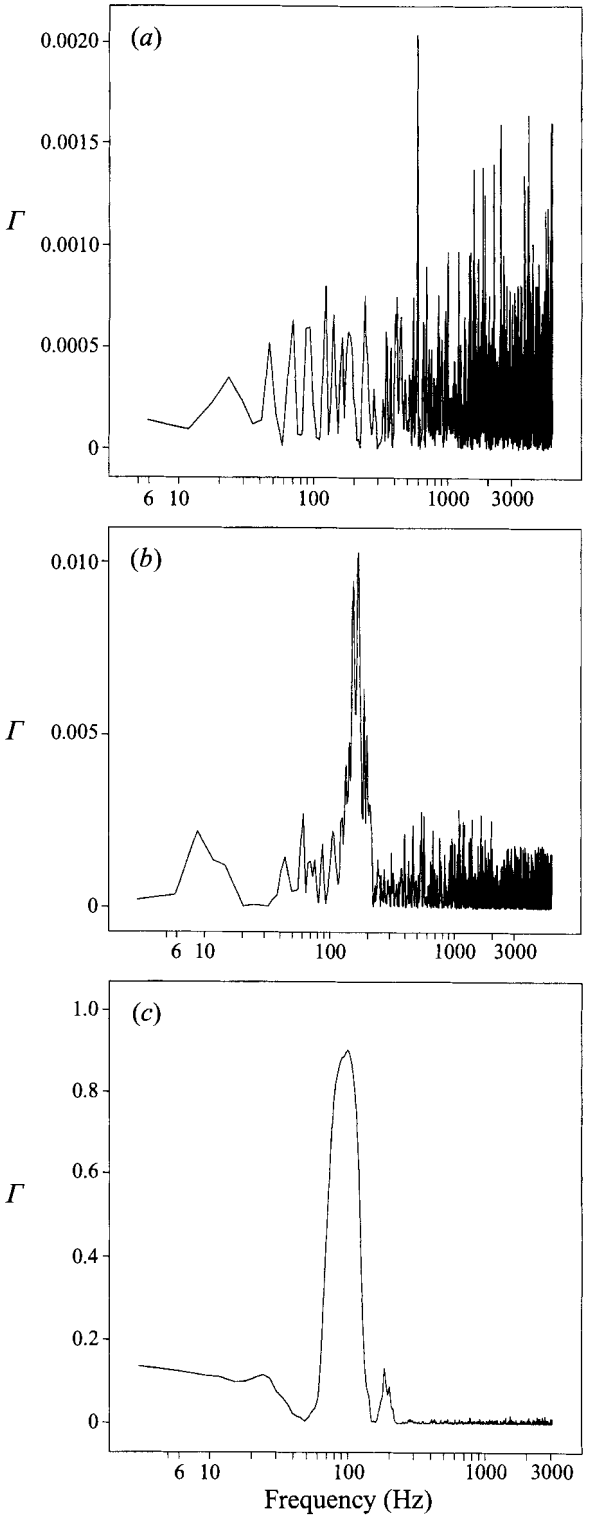

FIGURE 7. v–v coherence function for points at (*a*) $x = 1d$, $y = \pm 6$ mm; (*b*) $x = 5d$, $y = \pm 18$ mm; (*c*) $x = 24d$, $y = \pm 18$ mm.

frequency. From this we conclude that, at this streamwise location ($x = 15d$), the predominant broad-band peak at 100 Hz in the velocity spectra results from the quasi-periodic occurrence of large structures which have amalgamated from the smaller vortices. Considering that the periodicity becomes stronger at further downstream locations (figure 5*c*), we would expect that the small vortices within each large structure have become more closely assimilated, eventually merging completely. This vortex merging evidently plays an important role in the evolution of the wake.

There of course may be cases where the smaller vortices do not merge. Such isolated vortices would be expected to decay without adding anything to the evolution of the large structures.

3.3. *Interaction of the two shear layers*

In order to study the interaction of the two shear layers in more detail, two X-wire probes were positioned on the two opposite sides of the wake flow at different streamwise stations. Simultaneous two-point velocity measurements were performed, and the coherence function Γ was extracted,

$$\Gamma = \frac{|S_{12}|^2}{S_{11} S_{22}},$$

where S_{11} and S_{22} are the autospectra of the velocity signals at points 1 and 2 and S_{12} is the cross-spectrum of the two signals. Figure 7(*a*) shows the two-point v–v coherence functions for the lateral velocities at the streamwise location of $x = 1d$ ($y = \pm 6.0$ mm). Figures 7(*b*) and 7(*c*) show the v–v coherence functions for the velocities at $x = 5d$ and $24d$ respectively. The overall magnitude of the coherence function in figure 7(*a*) is quite small compared to corresponding data at further downstream locations (figures 7*b* and 7*c*). This indicates that there is very little correlation between velocity fluctuations in the two shear layers at $x = 1d$. (The rapid high-amplitude fluctuation of Γ beyond about 1000 Hz reflects noise in the process).

As expected, the flow development within the two shear layers is initially independent. It should be noticed, however, that there is a relatively high spike at a frequency of about 590 Hz in figure 7(*a*). The spike, although still small in magnitude, suggests that there is a weak connection between the lateral velocities in the two shear layers at $x = 1d$. It is useful to compare this coherence function with the corresponding autospectrum in figure 5(*b*). The frequency of the spike in figure 7(*c*) is approximately equal to half the characteristic frequency in the autospectrum, namely 1000 Hz. The dominant spike in the v–v coherence function becomes progressively larger at further downstream locations. Beyond $x = 5d$, the results show that the correlation between the two layers is very significant at the relevant characteristic frequency.

From the above we conclude that although small-scale vortices develop independently within each of the shear layers and occur at a high frequency, the initial communication between the two layers is characterized by a relatively lower frequency. These lower-frequency waves appear to play the primary role in the early interaction between the two layers.

It should be mentioned that the spectral characteristics of the porous-body wake are significantly different from those in a solid body wake. At $x = 5d$ in the wake of a flat plate, a strong spike can be identified in the low frequency of the v-spectrum and this frequency remains relatively unchanged over a large range of downstream locations.

3.4. *Numerical simulation of shear-layer interactions*

A two-dimensional numerical simulation, involving a discrete-vortex method similar to that used by Meiburg (1987), was performed in order to illustrate the nonlinear

developments and interaction of the two shear layers. Initially, each of the two shear layers is represented by a row of 2000 two-dimensional spanwise discrete vortex *blobs* with finite core radius. The two vortex layers are separated by 18.8 mm, so that the resulting u-velocity generated by the two layers will match approximately the measured velocity profile at $x = 1d$. The vorticity distribution of each vortex blob is defined as

$$\frac{\omega(r)}{\Gamma} = \frac{\alpha}{\pi\sigma^2} \frac{1}{(r^2/\sigma^2+\alpha)^2},$$

where the constant $\alpha = 0.413$, as was taken from Leonard (1980). The 'core radius' of the vortex blob, σ, is chosen as 1.5 mm, and the centres of the vortex blobs are initially distributed about $\Delta x = 0.08$ mm apart. The overlapping of these blobs produces a continuous vorticity distribution in the shear layers. The circulation of each blob is given by $\Gamma = \Delta x\,(U_1 - U_2)$, where U_1 and U_2 are the streamwise velocities on the two sides of a shear layer. The numerical technique is based on the Biot–Savart integral,

$$\boldsymbol{u}(x) = -\frac{1}{4\pi}\int \frac{(\boldsymbol{x}-\boldsymbol{x}')\times\boldsymbol{\omega}(\boldsymbol{x}')}{|\boldsymbol{x}-\boldsymbol{x}'|^3}\,\mathrm{d}V(\boldsymbol{x}').$$

The nonlinear evolution of the flow is calculated by evaluating the velocities of the vortex blobs at each time step and advancing them over a finite time step using a predictor–corrector integration scheme,

$$\boldsymbol{x}' = \boldsymbol{x}(t) + \boldsymbol{u}(\boldsymbol{x}, t)\,\Delta t,$$

$$\boldsymbol{x}(t+\Delta t) = \boldsymbol{x}(t) + 0.5(\boldsymbol{u}(\boldsymbol{x}, t) + \boldsymbol{u}'(\boldsymbol{x}'))\,\Delta t.$$

To separate the effect of downstream/upstream interaction, the present simulation was restricted to temporally developing shear layers with periodic boundary conditions in the streamwise direction. At the beginning of the simulation, one of the shear layers (the upper layer) is subjected to an initial perturbation derived from harmonic waves with several different frequencies,

$$y(x) = 0.2[\sin(2\pi x f_0) + 0.4\sin(2\pi f_0/2) + 0.1\sin(2\pi x f_0/4)],$$

where x and y are in mm. As can be seen in the above formula, this perturbation consists of a basic harmonic with a wavelength of $1/f_0 = 8$ mm, and two other harmonic waves with longer wavelengths and smaller amplitudes. In the physical flow, the initial perturbation probably arises from the grid turbulence of the screen and can be considered as the superposition of many Fourier components (as can be seen from the $x = 1d$ spectrum in figure 5*c*).

The vorticity iso-contours at different stages of the shear-layer evolution are presented in figure 8. The results indicate that an instability in the upper layer (due to an initial perturbation) leads to vortex sheet roll-up at a frequency of f_0. Subsequently, vortex merging occurs, such that the resulting characteristic frequency in the upper layer is $\leqslant f_0/2$. Subjected to the influence of the upper layer and its own self-induction, the lower layer also develops in the same fashion as the upper one, except that the vortex sheet roll-up in the lower layer occurs directly at the subharmonic frequency, $f_0/2$. The vortices in both layers continue to merge until they reach a meta-stable configuration.

Although the development of the two vortex layers depends on their interaction and their self-induction, the evolution of the initially unperturbed lower layer illustrates the

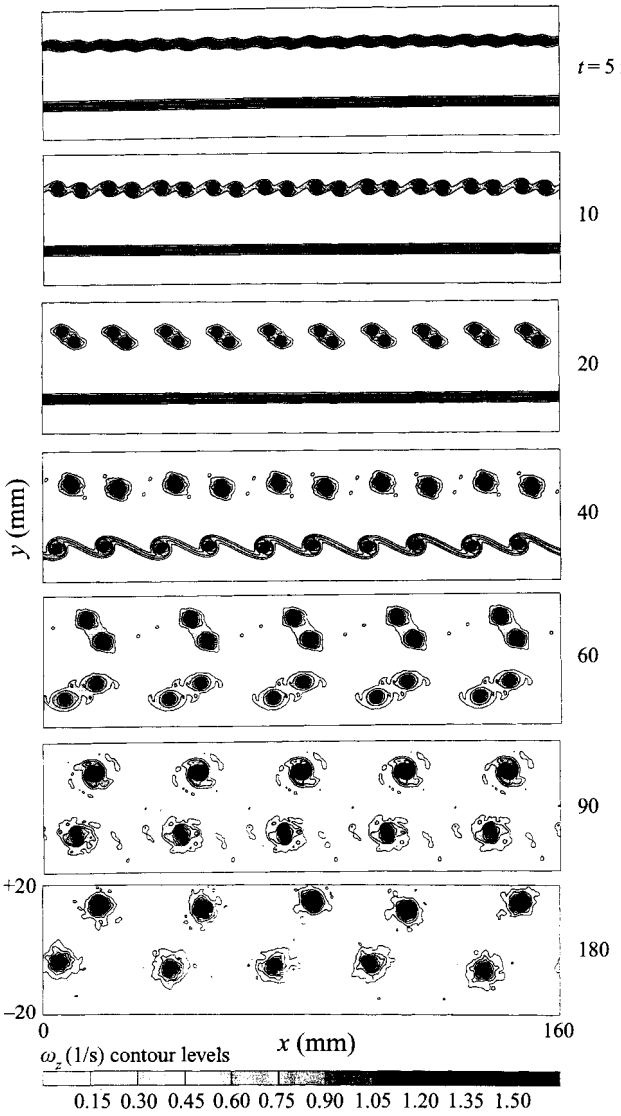

FIGURE 8. Vorticity iso-contours at different stages of simulated shear-layer evolution.

effect of one layer on the other, since, initially, the self-induction of the lower layer is small. Figure 9 depicts the shape of the two shear layers early in the development. It can be seen that while the upper layer is characterized by the basic frequency f_0, the lower layer, under the influence only of the upper one, is characterized by a much lower frequency. This result shows that the harmonic wave with the lowest frequency propagates most effectively to the other layer, even though that particular wave (with $f_0/4$) has the smallest amplitude.

It can be speculated from both experimental and numerical results that while the vortex sheet self-induction tends to amplify the perturbation of high frequencies, the interaction of two parallel vortex sheets tends to amplify the low-frequency perturbation. During the interaction of the two shear layers, the sub-harmonic wave or Fourier component is amplified, which could help synchronize the vortex pairing on the two sides.

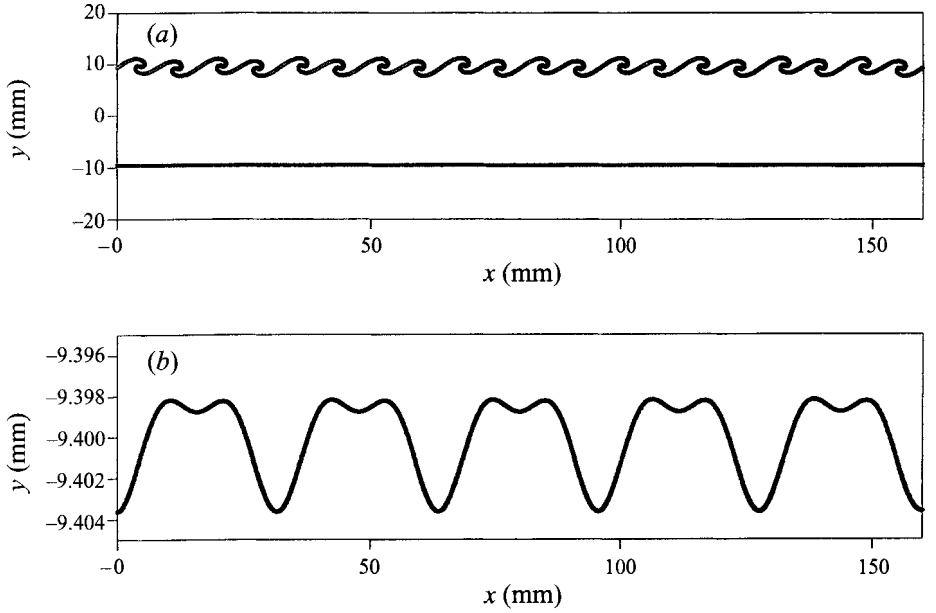

FIGURE 9. Positions of vortex centres in the simulated shear-layer evolution at $t = 10$ ms. (*a*) Overall view; (*b*) magnified view of lower layer; (*c*) v–v coherence function for points at $x = 24d$, $y = \pm 18.0$ mm.

4. Conclusions

Based on the experimental and numerical results and the above discussion, it can be concluded that the large-scale coherent spanwise structures in the near region ($20d < x < 30d$) of the porous-body wake are due to the merging and interaction of the small-scale vortices formed in the region *very close* to the screen ($x < 1d$). The two shear layers are able to communicate with each other, although they are physically separated by the much less-intensive turbulent core fluid in the centre.

This research was supported by the Natural Sciences and Engineering Research Council of Canada through Grant A-2746.

REFERENCES

BEVILAQUA, P. M. & LYKOUDIS, P. S. 1978 Turbulence memory in self-preserving wakes. *J. Fluid Mech.* **89**, 589–606.

CANTWELL, B. J. & COLES, D. 1983 An experimental study of entrainment and transport in the turbulent near wake of a circular cylinder. *J. Fluid Mech.* **136**, 321–374.

CASTRO, I. P. 1971 Wake characteristics of two-dimensional perforated plates normal to an air-stream. *J. Fluid Mech.* **46**, 599–609.

CIMBALA, J. M., NAGIB, H. M. & ROSHKO, A. 1988 Large structure in the far wakes of two-dimensional bluff bodies. *J. Fluid Mech.* **190**, 265–298.

INOUE, O. 1985 A new approach to flow problems past a porous plate. *AIAA J.* **23**, 1916–1921.

LEONARD, A. 1980 Vortex methods for flow simulation. *J. Comput. Phys.* **37**, 289–335.

LOUCHEZ, P. R., KAWALL, J. G. & KEFFER, J. F. 1987 Detailed spread characteristics of plane turbulent wakes. In *Turbulent Shear Flows 5* (ed. F. Durst, B. E. Launder, F. W. Schmidt & J. H. Whitelaw), p. 98. Springer.

MEIBURG, E. 1987 On the role of subharmonic perturbations in the far wake. *J. Fluid Mech.* **177**, 83–107.

PERRY, A. E. & STEINER, T. R. 1987 Large-scale vortex structures in turbulent wakes behind bluff bodies. *J. Fluid Mech.* **174**, 233–298.

ROSHKO, A. 1976 Structure of turbulent shear flows. *AIAA J.* **14**, 1349.

WYGNANSKI, I., CHAMPAGNE, F. & MARASLI, B. 1986 On the large-scale structures in two-dimensional, small-deficit, turbulent wakes. *J. Fluid Mech.* **168**, 31–71.

ZHOU, Y. & ANTONIA, R. A. 1994 Effect of initial conditions on vortices in a turbulent near wake. *AIAA J.* **32**, 1207.

ZUCHERMAN, L. 1988 Study of coherent structures within plane turbulent wakes using a pattern-recognition technique. PhD thesis, University of Toronto.